Wave-packet dynamics and edge transport in anomalous Floquet topological phases

Miguel F. Martínez [1,2] and F. Nur Ünal [2,*]

[1]*Department of Physics, KTH Royal Institute of Technology, 106 91 Stockholm, Sweden*

[2]*TCM Group, Cavendish Laboratory, University of Cambridge, JJ Thomson Avenue, Cambridge CB3 0HE, United Kingdom*

(Received 7 June 2023; revised 7 November 2023; accepted 7 November 2023; published 20 December 2023)

The possibility of attaining chiral edge modes under periodic driving has spurred tremendous attention both theoretically and experimentally, especially in light of anomalous Floquet topological phases that feature vanishing Chern numbers unlike any static counterpart. We consider here a periodically modulated honeycomb lattice and experimentally relevant driving protocols, which allows us to obtain edge modes of various character in a simple model. We calculate the phase diagram over a wide range of parameters and recover an anomalous topological phase with quasienergy gaps harboring edge states with opposite chirality. Motivated by the advances in single-site control in optical lattices, we investigate wave-packet dynamics localized at the edges in distinct Floquet topological regimes that cannot be achieved in equilibrium. We analyze transport properties in edge modes which originate from the same bands but with support at different quasienergies and sublattices as well as possessing different chiralities. We find that an anomalous Floquet topological phase can in general generate more robust chiral edge motion than a Haldane phase, allowing for more effective loading of the wave packet into edge channels. Our results demonstrate that the rich interplay of wave-packet dynamics and topological edge states can serve as a versatile tool in ultracold quantum gases in optical lattices.

DOI: 10.1103/PhysRevA.108.063314

I. INTRODUCTION

Topologically protected phenomena entail a prominent research direction in condensed-matter physics [1,2]. A wide range of novel phases arising from the interplay of topology and symmetries have been theorized and observed, with intriguing features being unearthed regularly especially in highly nontrivial many-body or out-of-equilibrium settings [3–19]. Regarding the latter, rapid developments have extended topological characterizations to periodically driven Floquet systems [20–25] and dynamic quench settings with new invariants [26–29], even reaching to exotic multigap topologies with non-Abelian braiding properties [30–36]. From an experimental point of view, Floquet engineering [37–39] has been established as a powerful tool to realize paradigmatic models in periodically driven nonequilibrium quantum matter in platforms such as ultracold atoms [25,40–43] and photonic lattices [44,45], allowing for not only a high degree of control and efficient quantum simulations but also exploring new regimes unattainable in equilibrium.

In a Floquet system, where energy is not a conserved quantity due to broken continuous-time-translation invariance, one can adopt a description in terms of a periodic quasienergy since discrete-time translations are still present. An effective quasienergy spectrum and the topological information are encoded by the time evolution over a period T. Upon evaluating stroboscopically [38], a quasienergy can be defined as phase eigenvalues of the time-evolution operator, namely, as $\varepsilon_n T \in [-\pi, \pi)$ for n bands, modulo 2π in a Floquet Brillouin zone (FBZ). The fact that quasienergy bands are phases forming a circle induces one additional, anomalous, π gap connecting the bands through the FBZ edge. The periodicity of the Floquet spectrum has paved the way for novel phases that truly arise from this out-of-equilibrium nature such as helical edge states crossing across the FBZ, anomalous Floquet Anderson insulators, and anomalous Dirac string phases [31,46,47].

Most interestingly, the possibility to obtain anomalous edge states in the FBZ-edge gap renders the equilibrium topological classification in terms of the Chern number C_n in two dimensions inept to characterize driven systems [22,23]. Rather than invariants of individual bands, one needs to consider winding numbers W_g associated with gaps centered around, e.g., $g = 0$ and $g = \pi$ for two levels. Consequently, the anomalous Floquet topological phase has attracted great attention, characterized by the winding number combination $[W_0, W_\pi] = [1, 1]$ harboring edge states in both gaps despite a vanishing Chern number [23,25]. Experimentally, individual edge modes have been probed in photonic lattices [44,45]. Advances in optical lattices have allowed for directly measuring the topological invariants [11,25,27] and in particular distinguishing the quasienergy gaps to unambiguously assign the observed winding numbers to individual gaps. However, coherent edge dynamics and transport properties in different quasienergy gaps, particularly with respect to each other and equilibrium phases, remain an open question. Recent

*fnu20@cam.ac.uk

advances in single-site accessibility [48] in optical lattices now offer new possibilities for the creation of sharp edges and probing topological edge modes by using localized wave packets to investigate unique Floquet topological features as well as the effect of different quasienergy gaps associated with different branch cuts.

In this work we consider a periodically driven two-band model in two dimensions that is also experimentally relevant and analyze transport properties in different quasienergy gaps focusing on the distinct Floquet nature [24,25]. We calculate the phase diagram over a wide range of parameters and contrast different driving protocols. Going beyond the anomalous [1,1] phase that was originally introduced, this allows us to reach an unexplored anomalous Floquet topological phase where a pair of edge states with opposite chiralities is induced in different gaps ($[W_0, W_\pi] = [\pm 1, \mp 1]$) supported by the same two bands with finite Chern number, which cannot be obtained in equilibrium. We investigate the wave-packet dynamics in various topological, and in particular anomalous, phases. We study populating edge modes at different quasienergies and with different winding numbers by applying kicks, controlling the shape of the wave packet, and examine their robustness and efficiency of preparation. Addressing chiral edge dynamics in different phases where only a single gap or both gaps harbor edge modes, we show that an anomalous Floquet topological phase can give rise to much more robust edge transport than equilibrium Chern insulating phases. We further analyze the effect of the Floquet gauge and the sublattice character of the edge states.

II. MODEL

We consider a honeycomb lattice in two dimensions with a Hamiltonian given by

$$\hat{H} = -\sum_{\langle i,j\rangle} J\hat{a}_i^\dagger \hat{a}_j + \frac{\Delta}{2}\sum_{i\in A}\hat{a}_i^\dagger\hat{a}_i - \frac{\Delta}{2}\sum_{i\in B}\hat{a}_i^\dagger\hat{a}_i, \qquad (1)$$

where $\hat{a}_i^\dagger$ ($\hat{a}_i$) creates (annihilates) a particle on lattice site i, with a nearest-neighbor tunneling strength J and an energy offset Δ between the two sublattices A and B. We will introduce the periodic driving via the modulation of the hopping amplitudes J_m for $m = 1, 2, 3$ along the three nearest-neighbor vectors $\boldsymbol{d}_1 = (0, -1)a$, $\boldsymbol{d}_2 = (-1/2, \sqrt{3}/2)a$, and $\boldsymbol{d}_3 = (1/2, \sqrt{3}/2)a$, where a is the nearest-neighbor distance. The Hamiltonian at a given time instance is diagonal with respect to quasimomentum $\boldsymbol{k}$ and hence can be written as

$$\hat{H}(\boldsymbol{k}, t) = -\sum_{m=1}^{3} J_m(t)[\cos(d_m\boldsymbol{k})\sigma_x + \sin(d_m\boldsymbol{k})\sigma_y] + \frac{\Delta}{2}\sigma_z, \qquad (2)$$

where $\boldsymbol{\sigma}$ are the Pauli matrices.

The driving protocols that we implement are of stepwise nature [22,23], which not only offers conceptual simplicity for our theoretical characterization, but are also experimentally relevant as they have been recently implemented in optical lattices [25] with a smoothed modulation [49]. Specifically, one period of the drive is divided in three even steps of length $T/3$. For the first driving scheme, the tunneling is allowed cyclically only along one of the three directions during each stage with amplitude J [23,24]. Second, we employ another protocol, where during the mth step, the tunneling $J_m = \lambda J$ is enhanced by a factor of λ, while the tunneling in the other two directions is kept fixed at J [22]. The first drive can be seen as a limiting case of the second one for $\lambda \to \infty$ and $J \to 0$ while keeping λJ fixed. We will illustrate in detail the difference between the two schemes in the following.

Since during each step of the driving cycle, the Hamiltonian (2) becomes time independent, $\hat{H}_m(\boldsymbol{k})$, for both driving protocols, the time-evolution operator at the end of one period can be written as

$$\hat{\mathcal{U}}(\boldsymbol{k}, T) = e^{-i\hat{H}_3(\boldsymbol{k})(T/3)}e^{-i\hat{H}_2(\boldsymbol{k})(T/3)}e^{-i\hat{H}_1(\boldsymbol{k})(T/3)} = e^{-i\hat{\mathcal{H}}_F(\boldsymbol{k})T}, \qquad (3)$$

where we set $\hbar = 1$ throughout this paper. This stroboscopic evolution is captured by the Floquet Hamiltonian $\hat{\mathcal{H}}_F(\boldsymbol{k})$, defining the quasienergy spectrum through $\hat{\mathcal{H}}_F(\boldsymbol{k})|\phi_n(\boldsymbol{k})\rangle = \varepsilon_n|\phi_n(\boldsymbol{k})\rangle$. The Berry curvature and the Chern numbers of these quasienergy bands are calculated using the Floquet eigenstates $\phi_n(\boldsymbol{k})$. These topological invariants in the two-dimensional momentum-space BZ have however been shown to be insufficient to capture the Floquet topology [23]. One instead needs to consider also the time evolution within the period $\hat{\mathcal{U}}(\boldsymbol{k}, t)$. In Floquet settings, the two bands can close and reopen in two distinct ways: in the quasienergy gaps at zero but also at π, corresponding to a change in the branch cut for defining $\hat{\mathcal{H}}_F(\boldsymbol{k})$, as opposed to one possibility in a static system. This quasienergy gap labeling originating from the time periodicity requires a topological characterization that employs winding numbers defined in the (k_x, k_y, t) space. Each gap closing induces a transfer of Berry curvature between the bands, leaving chiral edge states behind in their respective gaps characterized by finite winding numbers. When the transitions in zero and π gaps trivialize each other, we arrive at an anomalous Floquet topological phase with a vanishing Chern number [23]. The latter can in general be expressed as the difference of the winding numbers (net number of edge states in a gap factoring in their chiralities) above and below a band, $C_n = W_{n,\text{above}} - W_{n,\text{below}}$. In the Floquet case, the extra π gap renders the spectrum unbounded and hence offers more interesting possibilities.

III. PHASE DIAGRAMS

Figure 1 demonstrates the phase diagrams that we numerically calculate in our driven honeycomb models for a representative parameter range. The winding numbers can in general be computed using the time-evolution operator at every point in the $(2+1)$-dimensional parameter space [23], although this may prove computationally and experimentally demanding in most cases. Instead, we here employ an approach based on tracking the change of the winding numbers in each gap as introduced in Ref. [24] and successfully implemented in Ref. [25] to measure anomalous winding numbers. In particular, in the high-frequency regime we utilize the equilibrium topological classification based on Chern numbers with a trivial winding number in the π gap [24,50]. In the case of the second driving protocol, $\lambda = 1$ automatically satisfies the static definition. We depart from the topological invariants that we calculate for these initial parameters at high

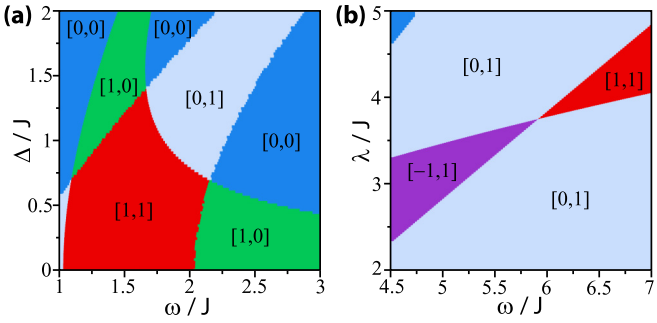

FIG. 1. Phase diagrams of the stepwise driven honeycomb lattice with corresponding winding numbers $[W_0, W_\pi]$. (a) First driving protocol with switching tunneling amplitudes along the three directions on and off completely, for modulation frequency ω and sublattice offset Δ. (b) Second protocol where tunneling amplitudes are cyclically enhanced by a factor of λ, with $\Delta = 2J$.

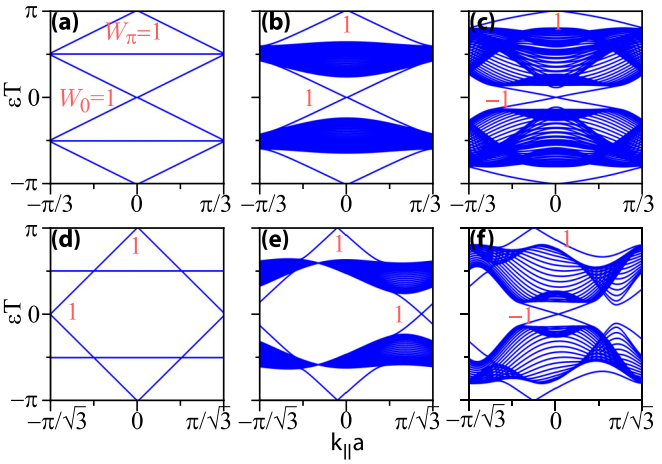

FIG. 2. Quasienergy spectra for a ribbon with [(a)–(c)] armchair and [(d)–(f)] zigzag terminations, with crystal momentum $k_\parallel$ in the periodic direction. In the [1,1] phase, here given for the first driving protocol introduced in the text, zero- and π-gap edge states occur well separated in momentum (a) and (d) at the fine-tuned point ($\omega = 4J/3$, $\Delta = 0$) and (b) and (e) ($\omega = 1.5J$, $\Delta = 0.5J$). (c) and (f) In the $[-1, 1]$ phase with the second driving scheme, the two edge states appear closer in momentum, for $\omega = 4.5J$, $\Delta = 2J$, and $\lambda = 3$.

frequencies for both driving protocols. As model parameters are being tuned, we compute the winding numbers, which change via band touching points in each gap, by evaluating the charge of these topological singularities in a gap-specific way (see the Supplemental Material for details [51]). The band singularities (hence edge modes) at the FBZ edge involve a change in the branch cut by π. We further confirm these winding numbers by computing the Hopf invariant at representative points in a given phase, which has been shown to equal the winding numbers [28].

For the first driving protocol where the tunneling amplitudes are cyclically turned on and off completely, the relevant tuning parameters are the sublattice offset and frequency. Indeed, this simple model illustrates a rich phase diagram including the previously predicted and observed anomalous Floquet topological phase [1,1] [see Fig. 1(a)], which can be understood by considering the limit of $\Delta = 0$ and $\omega = 4J/3$. For particles starting from one of the sublattices, this fine-tuned point corresponds to a complete population transfer to the other sublattice at the end of each step with tunneling allowed for a time of $JT/3 = \pi/2$. As we follow the driving cycle, it can be easily seen that particles in the bulk remain localized and only circularly move around each hexagon, ending up in alternating sublattice flavor at the end of each period and hence mixing the pseudospin character. However, in a finite system, particles move along the edge in a direction set by the chirality of the drive, corresponding to unit winding numbers of the same sign in both gaps despite the trivial invariant of the bulk bands.

The second driving scheme, on the other hand, provides one more knob to tune, namely, the driving amplitude λ. This allows for reaching more exotic phases, as we present in Fig. 1(b) as a function of λ and ω for a fixed sublattice offset $\Delta = 2J$. We identify a phase with winding numbers $[W_0, W_\pi] = [-1, 1]$, which we numerically verify to be inaccessible using the first driving protocol owing to the smaller number of tuning parameters in that case. Distinct from the previously introduced anomalous phase, this is a hitherto-unexplored anomalous Floquet topological phase that harbors edge states in both zero and the anomalous π gaps with *opposite chiralities*, supported by the same two bands. Hence, the lower (upper) band carries a Chern number $C_1 = -2$ ($C_2 = +2$). This anomalous phase is unique to the driven system, since in equilibrium there is only one gap where the topological transition can occur between the two bands (i.e. the zero gap). This gap could in principle host two edge modes of opposite chiralities also in the static case, provided they occur at two different quasimomenta. This would however correspond to vanishing Chern numbers of the two bands, making the anomalous $[-1, 1]$ phase exclusively emerging in the Floquet setting. Interestingly, these subtle differences also reflect on the edge transport and wave-packet dynamics, as will be illustrated subsequently.

IV. ANOMALOUS EDGE STATES

In order to investigate transport properties and chiral edge dynamics in different Floquet (anomalous) topological phases, we consider a ribbon geometry extended in the x direction, with N_y layers in the finite y direction. We present the edge spectra in Fig. 2 for both armchair and zigzag terminations. At the fine-tuned point within the [1,1] phase of the first driving protocol, the Floquet spectrum features completely flat bands corresponding to the localized bulk motion with extended edge modes crossing the entire FBZ [see Figs. 2(a) and 2(d)]. Although the armchair termination folds these two edge states to the same point, the zigzag spectrum reveals that the edge modes are well separated in momentum: While the zero-gap states form at the K point with finite momentum $\pi/\sqrt{3}$ in units of the lattice constant, π-gap states appear at the Γ point. We find that this is true in general in the [1,1] phase owing to the nature of band inversions required in this phase, also away from the fine-tuned case as illustrated in Figs. 2(b) and 2(e) with dispersive bands, as well as for the second driving protocol. Since armchair and zigzag terminations correspond to projecting along perpendicular directions in the momentum space, $k \to -k$ symmetry is naturally

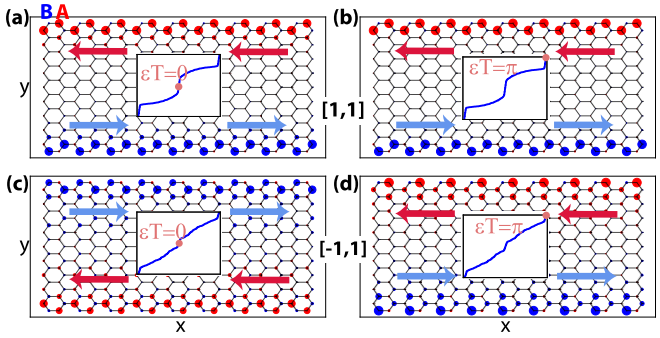

FIG. 3. Distribution of edge states at quasienergies (a) and (c) zero and (b) and (d) π, marked by dots in the insets on their corresponding quasienergy spectra, on a cylinder periodic in the x direction. (a) and (b) In the [1,1] phase with the same parameters as Fig. 2(b), both edge states are counterclockwise and localized at the same sublattices. (c) and (d) In the $[-1, 1]$ phase for the parameters given in Fig. 2(c), while the π-gap state localizes on A at the top edge, the zero-energy state with the opposite chirality localizes on the B sublattice.

broken in the presence of a finite sublattice offset for the latter [see Figs. 2(b) and 2(e)]. The edge modes nonetheless still carry a large momentum difference. On the contrary, in the $[-1, 1]$ phase in Figs. 2(c) and 2(f), the two edge modes with opposite chiralities appear closer in momentum, which will bring about an important distinction for the dynamics in the two anomalous phases.

The different chiralities of the edge states in the anomalous Floquet topological phases also affect their sublattice character as shown in Fig. 3. We here consider a cylinder geometry with periodic boundary conditions connecting N_x layers in the x direction. While in the [1,1] phase the counterclockwise edge states in the zero gap are localized on the A (B) sublattice on the upper (lower) end of the cylinder, the π-gap states support the same chiral motion localized on the same sublattice flavors. In the case of $[W_0, W_\pi] = [-1, 1]$, however, the system harbors both clockwise and counterclockwise edge modes. Figures 3(c) and 3(d) demonstrate that this is facilitated by swapping of the sublattice character of the zero-gap states along with their chirality. Hence, on the upper and lower ends of the cylinder, the two edge modes support opposite currents in different sublattices. Interestingly, the layers where zero- and π-gap currents have maximum density, depicted by the size of the circles, are also different. We emphasize that these two chiral modes do not hybridize despite being on the same edge as they are well separated in quasienergy. We now analyze how the interplay between the edge modes located at different momentum, quasienergy, and sublattices and with different chiralities affect their transport properties, especially with respect to each other and in different Floquet (anomalous) topological phases.

V. WAVE-PACKET DYNAMICS IN ANOMALOUS TOPOLOGICAL PHASES

Ultracold atomic systems have recently enjoyed rapid advances in single-site accessibility and local control with techniques such as quantum gas microscopes and optical tweezers [48,52–54]. Giving access to the creation of sharp edges, these pose a timely question and offer new opportunities for investigating wave-packet dynamics localized at the edges of a topological system as a powerful tool in optical lattices. The models that we implement allow us to retrieve a rich phase diagram within a simple geometry, where we compare edge transport in the conventional Haldane ([1,0]) [55] and Haldane-like phases ([0,1]), which are gauge equivalent, with the anomalous Floquet topological phase ([1,1]). Indeed, we show that edge state population in a given gap can be mostly controlled by employing appropriate kicks. Most importantly, we find that the [1,1] phase allows for a more robust chiral edge motion than the Haldane phases. We analyze the effects of opposite chiralities with the opportunity provided by the second anomalous phase ($[-1, 1]$) and the simultaneous activation of both edge modes giving rise to interesting chiral edge dynamics.

We consider a cylindrical geometry of $N_x \times N_y$ layers and a Gaussian wave packet, $\Psi(x, y) = \exp\{-(x - x_0)^2/4\sigma_x^2 - (y - y_0)^2/4\sigma_y^2 + iq_x x + iq_y y\}/\mathcal{N}$, initially localized at the upper edge [see the inset in Fig. 4(e)], at (x_0, y_0) with a spread given by (σ_x, σ_y) and normalization $\mathcal{N}$. We allow for an initial kick with momentum $\boldsymbol{q} = (q_x, q_y)$ which can be applied to control the overlap of the wave packet with edge states that are projected from the specified momenta onto the edge. We numerically calculate the evolution of the wave packet and present the probability at the edge sites in the upper two layers. In the [1,1] phase, a wave packet without any kick ($\boldsymbol{q} = 0$) predominantly overlaps with the π-gap states in Figs. 4(e) and 4(f), at and away from the fine-tuned point, since these edge states form at the Γ point (cf. Fig. 2). The corresponding wave-packet dynamics displays a clear chiral motion for long times around the edge of the cylinder which is periodic in the x direction. While some of the probability naturally disperses into the bulk for the dispersive [1,1] phase [see Fig. 4(b)], at the fine-tuned point the edge states are exclusively localized at A sublattices. The probability at B sites hence follows a chiral motion around each hexagon with completely flat bulk bands, giving rise to some probability dwelling around the initial position at all times in Fig. 4(a).

Due to the large separation of the zero- and π-gap states in the [1,1] phase, we can populate the edge modes at the zero gap by applying an initial kick of amount $|\boldsymbol{q}| = |K|$ to the wave packet. Figures 4(c) and 4(g) display a similar chiral motion with the not-kicked wave packet that is visibly indistinguishable, which is now mainly supported by the zero-gap states. We note that the kick direction (along the chiral edge mode or opposite to it) in fact does not matter as it only gives an overall phase, where the overlaps with eigenstates do not change and we observe the same dynamics. Moreover, since these wave packets are well localized in position space, we still obtain some spurious probability at the other gap, with or without a kick. This originates from the extensive overlap of the edge modes from the two gaps in position space [see Figs. 3(a) and 3(b)], despite the fact that they are well separated in momentum. Nevertheless, in both cases, we can control the chiral motion to be carried predominantly by the target quasienergy-gap modes. This shows that although these edge modes form at different gaps and despite the difference in the branch cuts by π while defining them, the wave packets

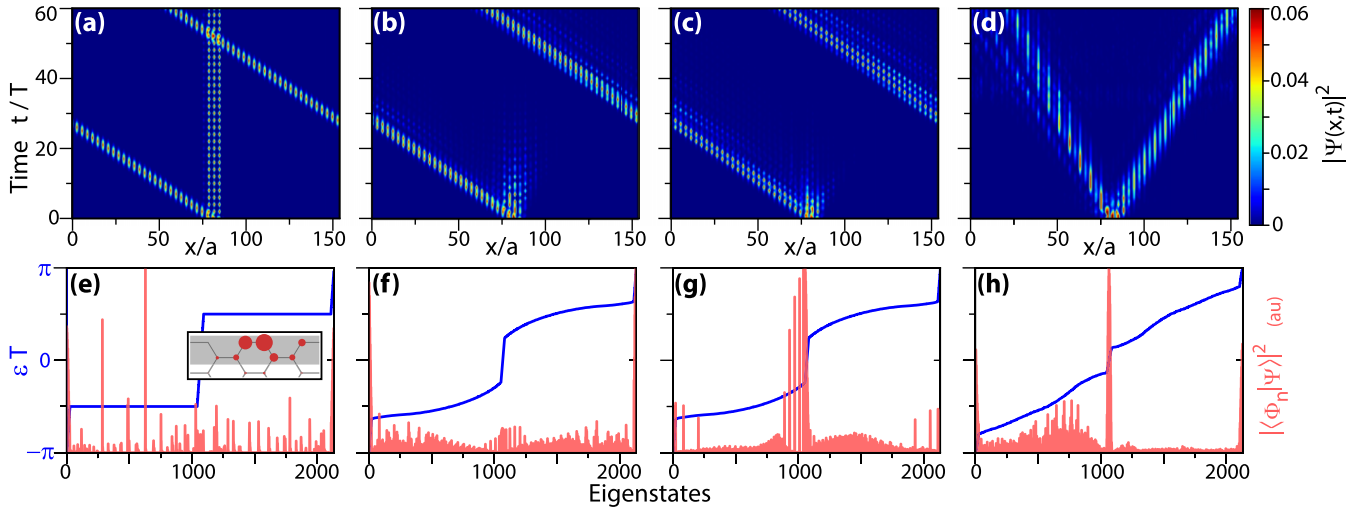

FIG. 4. [(e)–(h)] Overlap of a wave packet with the Floquet eigenstates and [(a)–(d)] its evolution at the edge sites (shaded two layers in the inset) on a cylinder periodic along x direction with $N_x = 104$ and $N_y = 41$ layers. The initial wave packets have $\sigma_x = 1$ and $\sigma_y = 0.5$, as depicted in the inset, where the radius of the circles is proportional to the initial probability at each site. (a) and (e) The [1,1] phase at the fine-tuned point. The wave packet initialized without a kick follows a clear chiral motion. For the [1,1] phase for the same parameters as in Fig. 2(b), the wave packet is initially given (b) and (f) a small kick $\boldsymbol{q} = (-0.17, 0)$ and (c) and (g) a larger kick $\boldsymbol{q} = (1.56, 0)$, to target the Dirac cones at the π and zero gaps, respectively. As revealed by the overlaps, applying appropriate kicks allows us to mainly populate a given gap, where the dynamics evolve similarly. (d) and (h) The $[-1, 1]$ phase for the same parameters as in Fig. 2(c). We now can largely populate both gaps simultaneously without a kick since the opposite chirality edge modes appear closer in momentum. The wave packet separates into two, giving rise to topologically protected currents traveling in both directions at the edge, with the Chern number ($|C| = 2$) corresponding to the difference of them.

can be controlled to populate mainly a given edge mode by applying appropriate kicks depending on their localization in quasimomentum rather than quasienergy. We present wider wave packets in the Supplemental Material [51] where the population of a given gap can be further increased, which could be experimentally realized, for example, by scanning a wider region with the laser initializing the wave packets.

On the other hand, in the $[-1, 1]$ phase achievable with the second driving protocol, both zero and π gaps harbor edge modes, but their separation in momentum is less pronounced. Both edge modes can then be extensively populated with the same wave packet, as demonstrated in Fig. 4(h), without applying any kick. Distinctively, since the winding numbers have opposite signs, we observe that the wave packet separates into two [see Fig. 4(d)], with a topologically protected current going in both directions at the edge of the cylinder, where the π modes travel slightly faster in accordance with the spectrum [cf. Figs. 2(c) and 2(f)]. We emphasize that in this phase, the quasienergy bands carry a Chern number $|C| = 2$, which is visible in the difference of the chiral currents at the edge of the system, rather than two topologically protected channels traveling in the same direction that would be expected in a static setting.

The anomalous Floquet topological phases carry distinct features arising from their out-of-equilibrium nature. First of all, both edge modes behave effectively as one single channel in the [1,1] phase due to their similar chirality. It is hence instructive to explore whether this anomalous Floquet topological phase (with two edge states of the same chirality at different quasienergy gaps) gives rise to an edge transport different from the Haldane phases with a single chiral mode, i.e., to contrast anomalous Floquet topological phases with the equilibrium Chern insulating phases. We demonstrate the wave-packet dynamics in the [1,0] and [0,1] phases in Figs. 5(a) and 5(b), respectively. While we apply a kick ($\boldsymbol{q} = K$) to the wave packet to target the zero-gap states in [1,0] as they form at the K point, we generally obtain a chiral transport at the edge, as expected in both phases.

Most importantly, upon comparing with the Haldane phases as visible in their color scales, we observe that the wave-packet dynamics in the anomalous Floquet phase [1,1] is much more robust, with the edge separating more from the bulk. To quantify this finding, we consider cuts on the phase diagram [Fig. 1(a)] across different phases and evaluate the total overlap of a wave packet with the edge states in Figs. 5(c) and 5(d). Targeting the zero-gap states with a kick, we indeed find that the total percentage of the edge state population is overall much higher in the [1,1] phase than in the [1,0] phase, where the former comprises mostly zero-gap states that are further enhanced by the π-gap contribution [see Fig. 5(c)]. Similarly, Fig. 5(d) shows that the wave packet, now initialized without a kick, overlaps with the π-gap states much more in [1,1] than in [0,1], where the zero-gap states further strengthen the edge dynamics in the former. We observe that this behavior is in general present across the phase diagram and also for the second driving protocol.

Remarkably, this demonstrates that a wave packet can be prepared to populate the edge modes more easily and efficiently in the anomalous phase than in Haldane phases. The anomalous topological phase then supports a more pronounced chiral edge motion with less leakage into the bulk. The more robust edge transport in the anomalous Floquet phase stems from the fact that the edge of the system accommodates two different channels rather than one, increasing the

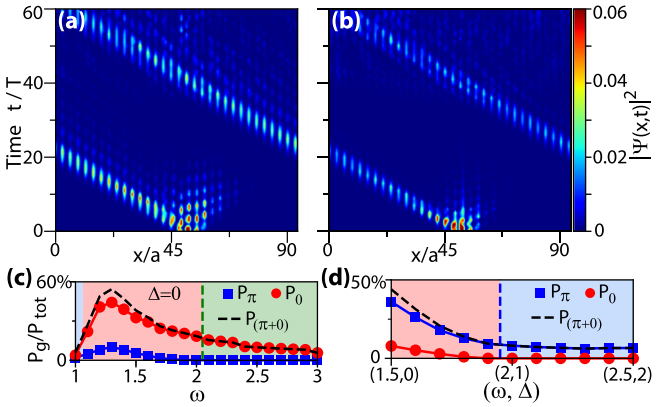

FIG. 5. Edge dynamics of a wave packet (a) with an initial kick $\boldsymbol{q} = (\pi/\sqrt{3}, 0)$ in the [1,0] phase for $\omega = 2.2J$ and $\Delta = 0$ and (b) without a kick in the [0,1] phase for $\omega = 2J$ and $\Delta = 1J$. Both dynamics in the Haldane phases show qualitative differences from Figs. [4(a)–4(c)], as they are less pronounced. (c) Percentage of the total probability carried by edge states in each gap, along the $\Delta = 0$ cut of Fig. 1(a) crossing different phases. The edge state population is much higher in the [1,1] phase (red shaded area) than in the [1,0] phase (green shaded area), for a wave packet with an initial kick as in (a) to target zero-gap states. (d) Similarly, the total probability per gap along a diagonal cut on the phase diagram crossing from [1,1] to [0,1], where the wave packet is given a small initial momentum to target the π-gap states forming close to Γ. A greater probability is supported by the two edge channels in the [1,1] phase along both cuts (c) and (d), quantifying that edge transport is overall more robust in the anomalous phase.

relative weight of the edge channels compared to the bulk so that they better separate spatially. Compared to the topological phases with equilibrium counterparts, there is one more gap available to harbor edge states in the anomalous Floquet topological phase, which renders stronger edge transport possible, supported with more edge states in the driven system. This can also aid novel anomalous Floquet Anderson phases under disorder [47]. We note that this qualitative analysis naturally depends on system details such as the bulk gap width and the properties of the phase. Indeed, we also obtain that the total edge population by a wave packet is overall larger for the $[-1, 1]$ phase than the Haldane-like phase (see the Supplemental Material [51]). Although the trend is less pronounced due to different chiralities and parameter dependences, the effect is still clearly discernible when the anomalous phase harbors two edge channels.

The anomalous Floquet phase $[-1, 1]$ manifests appealing features as well with the edge transport of opposite chiralities supported by the same bands. Since these edge modes are located at different quasienergy gaps and have support on different sublattices, they do not hybridize as demonstrated in Fig. 6(a). When we consider a cylinder with a smaller size, we confirm that the opposite-going currents at the edge circle the cylinder and pass through each other without disruption for several cycles. Similarly, when we introduce two wave packets, the crossing of the edge currents is clearly visible in Fig. 6(b). We note that introducing two wave packets is an experimentally promising route for probing these anomalous topological dynamics with opposite chiralities, where

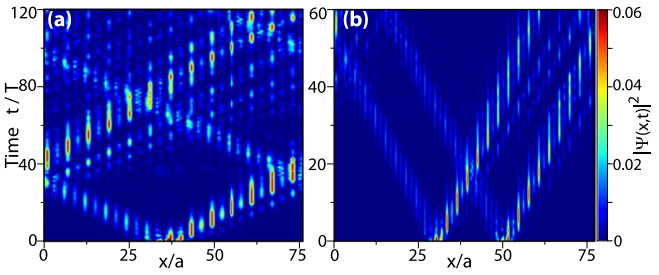

FIG. 6. In the $[-1, 1]$ phase with the parameters in Fig. 2(c), the wave packet is initialized without a kick on a smaller cylinder with $N_x = 52$ and $N_y = 41$. (a) Opposite going currents circle the cylinder and cross without disruption. (b) Two wave packets initialized at the edge pass through each other without hybridizing as they are well separated in quasienergy.

localized particles can be created around circular-shaped sharp edges punched in a system with laser potentials.

Although the analysis carried out here is generic for any parameters in a given phase, the particular details of different edge currents depend on various aspects. For example, we observe some tails developing and traveling with different velocities in some dynamics. This generally arises when many momentum states are stimulated due to the finite size of the wave packet, where the velocity of a given edge mode might be different at different quasimomenta (cf. Fig. 2) as well as different velocities that can be associated with different edge modes. We analyze some important details that can give rise to varying edge dynamics in a real system next.

VI. FLOQUET GAUGE AND SUBLATTICE DEPENDENCE

For the wave-packet dynamics presented in previous sections, we numerically calculate the time evolution by employing the Floquet Hamiltonian given in Eq. (3). While such stroboscopic definitions are useful, we verify that these dynamic features are overall reproduced also by following the exact time evolution under the two driving protocols, justifying the employment of an effective description neglecting the micromotion [38]. Although here we set the initial time to zero ($t_0 = 0$) for simplicity, the time-evolution operator and hence the Floquet Hamiltonian in Eq. (3) actually depend on this so-called Floquet gauge $\hat{\mathcal{H}}_F^{t_0}(\boldsymbol{k})$ as well as the Floquet eigenstates [38,39].

The Floquet gauge can influence the wave-packet dynamics in experiments especially at lower frequencies where the details within a period become more crucial. We elucidate this by considering the extreme limits of a wave packet completely localized on an A site at the upper edge in Fig. 7(a) and the fined-tuned point in the first driving protocol, where we obtain complete population transfer between sublattices at the end of each step of the drive. When we start from $t_0 = 0$ with the tunneling amplitudes turned on and off cyclically as $J_1 \to J_2 \to J_3$, particles move along the edge leftward. However, if we consider another initial time, e.g., $t_0 = T/3$, within the same sequence (i.e., $J_2 \to J_3 \to J_1$), particles would follow a chiral bulk motion around the hexagon. Away from the fine-tuned point, eigenstates mix sublattice flavors at varying degrees, but the Floquet gauge dependence remains. While this can give

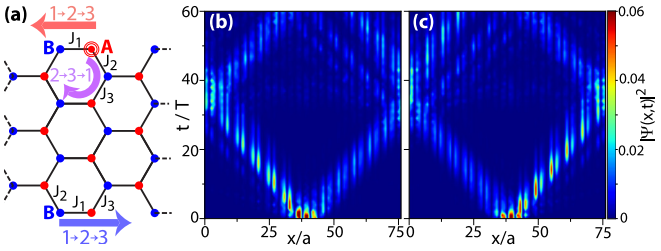

FIG. 7. (a) Illustration of the relation between the upper or lower edge dynamics and the sublattice character by considering the fine-tuned point of the first driving protocol. Starting from $t_0 = 0$ and following the chiral motion with $J_1 \to J_2 \to J_3$ turned on cyclically, a particle localized on sublattice A at the upper edge moves along the edge leftward (red arrow). Starting from a different initial time of $t_0 = T/3$ induces a bulk motion around the hexagon (purple). At the lower edge, the sublattice characters giving rise to the edge and bulk motions are swapped, which starting from B at $t_0 = 0$ generates edge motion (blue). (b) and (c) Dynamics on a cylinder in the $[-1, 1]$ phase for the same parameters as in Fig. 2(c), where we localize the wave packet without a kick at the same x position on the upper and lower edges, respectively. We average over 20 equally spaced initial times t_0 within a period, which produce similar chiral motion.

rise to some modifications in the exact dynamics observed, it does not alter our general conclusions. Furthermore, this is naturally less pronounced for more balanced or wider wave packets.

The upper and lower edges of the system may give rise to different dynamics as well, since the pseudospin character reflects oppositely on these two physical edges. Specifically, the chiral edge motion observed at the upper edge when we start from the sublattice A as depicted in Fig. 7(a) can be obtained at the bottom edge starting from the sublattice B (and similarly for the bulk localized states). When $\Delta = 0$, the Hamiltonian can be cast into a diagonal form in the pseudospin. The up spin in the upper edge corresponds to the down spin at the lower edge, which hence can bring about different dynamics depending on their population by the wave packet. While in general for $\Delta \neq 0$ the spin characters are mixed, they are mixed in the same but opposite way at the upper and lower edges, i.e., some up-down mixture on one end corresponds to the opposite down-up mixture on the other end. Changing the sign of the offset $\Delta \to -\Delta$ then inverts the upper-lower edge character, which we confirm in our numerics.

Overall, when we average out over various dynamics, the upper and lower ends of the system naturally give rise to the same behavior as it samples through different initial times and sublattice characters. We consider a wave packet localized in the same way at the upper and lower edges of a cylinder, at the same x positions in the geometry depicted in Fig. 7(a). We numerically calculate the chiral edge currents starting from different t_0 initial times (for 20 data points equally spaced over one period) which correspond to different eigenstates. We demonstrate the average wave-packet dynamics at the respective edges in Figs. 7(b) and 7(c). While the upper and lower edge dynamics might be very different at a given t_0, we observe that the π-gap states generate the similar leftward and rightward currents at the top and bottom edges on average as expected, as well as the zero-gap modes supporting opposite chirality. We note that the negligible difference between the upper and lower dynamics in the figure stems from the coarse sampling for averaging, where more data points wash out these differences further.

VII. CONCLUSION

In this work, we focused on the topological edge transport and chiral motion at the edge of a periodically driven system, particularly in anomalous Floquet topological phases unique to these out-of-equilibrium settings [22,23]. In light of recent developments in single-site accessibility in optical lattices, which offers the possibility to probe the dynamics locally at sharp edges, we investigated wave-packet dynamics as a versatile tool in exploring topologically protected Floquet edge modes. We considered a honeycomb lattice under experimentally relevant and conceptually insightful stepwise modulated driving protocols [24,25], which allowed us to retrieve a rich phase diagram, involving the conventional Haldane(-like) phases that can be realized in equilibrium as well as two different anomalous Floquet topological phases with no static counterparts that harbor edge states of different chiralities in both quasienergy gaps.

We showed that, in the [1,1] phase, the edge modes in different quasienergies behave predominantly like a single channel with the same chirality and sublattice character, where wave packets can be controlled to mostly populate one of the gaps by applying appropriate kicks as they are well separated in momentum. While this behavior is similar to the Haldane phases with a topologically protected edge mode present only in a single gap [55], we found that the anomalous [1,1] phase can generally support a more robust edge transport with edge states separating more from the bulk. We explained this by having two different channels coming from both gaps accommodated at the edge of the system, which enhances the population of the edge modes by the wave packets, providing an overall advantage over Haldane phases with equilibrium counterparts.

We further showed an anomalous phase with opposite winding numbers $[-1, 1]$ that can be achieved using the second driving protocol in a honeycomb lattice, where the system features both clockwise and counterclockwise currents now carried mainly by different sublattices at a given edge. Since the edge modes of opposite chiralities form much closer in momentum, we observed that wave packets localized at the edge largely populate both channels, which generates two independent currents going in opposite ways that can transverse through one another without hybridizing. We also analyzed the dependence of the dynamics on the details of the drive and the exact position where the wave packets are localized. We discussed that these effects can be controlled by changing the shape of the wave packet or averaging over different initial times. Our results demonstrate that investigating Floquet topological edge modes by using wave packets in optical lattices can reveal unique out-of-equilibrium features. These insights can be also employed in phases involving a larger number of edge states and with different chirality combinations [56], which might reveal more

interesting edge dynamics and more robust edge transport engaging multiple edge channels. Photonic lattices employing quantum walks offer another promising route to study various anomalous Floquet phases with different winding number combinations [57].

Note added. Recently, we became aware of related experimental work studying and probing wave-packet dynamics in an anomalous Floquet topological phase, which has been reported in Ref. [53].

Data sharing is not applicable to this article as no data sets were generated or analyzed during the present study.

ACKNOWLEDGMENTS

We thank Nigel Cooper and Robert-Jan Slager, for insightful discussions and comments on the manuscript, as well as the experimental team Monika Aidelsburger, Raphaël Saint-Jalm, Christoph Braun, Alexander Hesse, and Johannes Arceri. F.N.Ü. acknowledges funding from the Royal Society under a Newton International Fellowship, the Marie Skłodowska-Curie program of the European Commission Grant No. 893915, and Trinity College Cambridge. This work received funding from the European Research Council under the European Union's Horizon 2020 research and innovation program (Grant Agreement No. 101001902).

[1] M. Z. Hasan and C. L. Kane, *Colloquium*: Topological insulators, Rev. Mod. Phys. **82**, 3045 (2010).
[2] X.-L. Qi and S.-C. Zhang, Topological insulators and superconductors, Rev. Mod. Phys. **83**, 1057 (2011).
[3] D. J. Thouless, M. Kohmoto, M. P. Nightingale, and M. den Nijs, Quantized Hall conductance in a two-dimensional periodic potential, Phys. Rev. Lett. **49**, 405 (1982).
[4] B. A. Bernevig, T. L. Hughes, and S.-C. Zhang, Quantum spin Hall effect and topological phase transition in HgTe quantum wells, Science **314**, 1757 (2006).
[5] C. Fang, M. J. Gilbert, and B. A. Bernevig, Bulk topological invariants in noninteracting point group symmetric insulators, Phys. Rev. B **86**, 115112 (2012).
[6] C. L. Kane and E. J. Mele, Z_2 topological order and the quantum spin Hall effect, Phys. Rev. Lett. **95**, 146802 (2005).
[7] R.-J. Slager, A. Mesaros, V. Juričić, and J. Zaanen, The space group classification of topological band-insulators, Nat. Phys. **9**, 98 (2013).
[8] J. Kruthoff, J. de Boer, J. van Wezel, C. L. Kane, and R.-J. Slager, Topological classification of crystalline insulators through band structure combinatorics, Phys. Rev. X **7**, 041069 (2017).
[9] H. C. Po, A. Vishwanath, and H. Watanabe, Symmetry-based indicators of band topology in the 230 space groups, Nat. Commun. **8**, 50 (2017).
[10] B. Bradlyn, L. Elcoro, J. Cano, M. G. Vergniory, Z. Wang, C. Felser, M. I. Aroyo, and B. A. Bernevig, Topological quantum chemistry, Nature (London) **547**, 298 (2017).
[11] G. Jotzu, M. Messer, R. Desbuquois, M. Lebrat, T. Uehlinger, D. Greif, and T. Esslinger, Experimental realization of the topological Haldane model with ultracold fermions, Nature (London) **515**, 237 (2014).
[12] M. Aidelsburger, M. Lohse, C. Schweizer, M. Atala, J. T. Barreiro, S. Nascimbene, N. R. Cooper, I. Bloch, and N. Goldman, Measuring the Chern number of Hofstadter bands with ultracold bosonic atoms, Nat. Phys. **11**, 162 (2015).
[13] D. T. Tran, A. Dauphin, A. G. Grushin, P. Zoller, and N. Goldman, Probing topology by "heating": Quantized circular dichroism in ultracold atoms, Sci. Adv. **3**, e1701207 (2017).
[14] L. Asteria, D. T. Tran, T. Ozawa, M. Tarnowski, B. S. Rem, N. Flashner, K. Sengstock, N. Goldman, and C. Weitenberg, Measuring quantized circular dichroism in ultracold topological matter, Nat. Phys. **15**, 449 (2019).
[15] C. J. D. Kemp, N. R. Cooper, and F. N. Ünal, Nested-sphere description of the n-level chern number and the generalized Bloch hypersphere, Phys. Rev. Res. **4**, 023120 (2022).
[16] X. Tan, D.-W. Zhang, Z. Yang, J. Chu, Y.-Q. Zhu, D. Li, X. Yang, S. Song, Z. Han, Z. Li, Y. Dong, H.-F. Yu, H. Yan, S.-L. Zhu, and Y. Yu, Experimental measurement of the quantum metric tensor and related topological phase transition with a superconducting qubit, Phys. Rev. Lett. **122**, 210401 (2019).
[17] P. Xu, W. Zheng, and H. Zhai, Topological micromotion of Floquet quantum systems, Phys. Rev. B **105**, 045139 (2022).
[18] M. Jangjan, L. E. F. Foa Torres, and M. V. Hosseini, Floquet topological phase transitions in a periodically quenched dimer, Phys. Rev. B **106**, 224306 (2022).
[19] M. Jangjan and M. V. Hosseini, Floquet engineering of topological metal states and hybridization of edge states with bulk states in dimerized two-leg ladders, Sci. Rep. **10**, 14256 (2020).
[20] R. Roy and F. Harper, Periodic table for Floquet topological insulators, Phys. Rev. B **96**, 155118 (2017).
[21] T. Oka and H. Aoki, Photovoltaic Hall effect in graphene, Phys. Rev. B **79**, 081406(R) (2009).
[22] T. Kitagawa, E. Berg, M. Rudner, and E. Demler, Topological characterization of periodically driven quantum systems, Phys. Rev. B **82**, 235114 (2010).
[23] M. S. Rudner, N. H. Lindner, E. Berg, and M. Levin, Anomalous edge states and the bulk-edge correspondence for periodically driven two-dimensional systems, Phys. Rev. X **3**, 031005 (2013).
[24] F. N. Ünal, B. Seradjeh, and A. Eckardt, How to directly measure Floquet topological invariants in optical lattices, Phys. Rev. Lett. **122**, 253601 (2019).
[25] K. Wintersperger, C. Braun, F. N. Ünal, A. Eckardt, M. D. Liberto, N. Goldman, I. Bloch, and M. Aidelsburger, Realization of an anomalous Floquet topological system with ultracold atoms, Nat. Phys. **16**, 1058 (2020).
[26] C. Wang, P. Zhang, X. Chen, J. Yu, and H. Zhai, Scheme to measure the topological number of a Chern insulator from quench dynamics, Phys. Rev. Lett. **118**, 185701 (2017).
[27] M. Tarnowski, F. N. Ünal, N. Fläschner, B. S. Rem, A. Eckardt, K. Sengstock, and C. Weitenberg, Measuring topology from dynamics by obtaining the Chern number from a linking number, Nat. Commun. **10**, 1728 (2019).

[28] F. N. Ünal, A. Eckardt, and R.-J. Slager, Hopf characterization of two-dimensional Floquet topological insulators, Phys. Rev. Res. **1**, 022003(R) (2019).
[29] H. Hu and E. Zhao, Topological invariants for quantum quench dynamics from unitary evolution, Phys. Rev. Lett. **124**, 160402 (2020).
[30] F. N. Ünal, A. Bouhon, and R.-J. Slager, Topological euler class as a dynamical observable in optical lattices, Phys. Rev. Lett. **125**, 053601 (2020).
[31] R.-J. Slager, A. Bouhon, and F. N. Ünal, Floquet multi-gap topology: Non-Abelian braiding and anomalous dirac string phase, arXiv:2208.12824.
[32] J. Ahn, S. Park, and B.-J. Yang, Failure of Nielsen-Ninomiya theorem and fragile topology in two-dimensional systems with space-time inversion symmetry: Application to twisted bilayer graphene at magic angle, Phys. Rev. X **9**, 021013 (2019).
[33] A. Bouhon, Q. Wu, R.-J. Slager, H. Weng, O. V. Yazyev, and T. Bzdušek, Non-Abelian reciprocal braiding of Weyl points and its manifestation in ZrTe, Nat. Phys. **16**, 1137 (2020).
[34] A. Bouhon, T. Bzdušek, and R.-J. Slager, Geometric approach to fragile topology beyond symmetry indicators, Phys. Rev. B **102**, 115135 (2020).
[35] B. Jiang, A. Bouhon, Z.-K. Lin, X. Zhou, B. Hou, F. Li, R.-J. Slager, and J.-H. Jiang, Experimental observation of non-Abelian topological acoustic semimetals and their phase transitions, Nat. Phys. **17**, 1239 (2021).
[36] T. Jiang, Q. Guo, R.-Y. Zhang, Z.-Q. Zhang, B. Yang, and C. T. Chan, Four-band non-Abelian topological insulator and its experimental realization, Nat. Commun. **12**, 6471 (2021).
[37] N. Goldman and J. Dalibard, Periodically driven quantum systems: Effective Hamiltonians and engineered gauge fields, Phys. Rev. X **4**, 031027 (2014).
[38] A. Eckardt, *Colloquium*: Atomic quantum gases in periodically driven optical lattices, Rev. Mod. Phys. **89**, 011004 (2017).
[39] M. Bukov, L. D'Alessio, and A. Polkovnikov, Universal high-frequency behavior of periodically driven systems: From dynamical stabilization to Floquet engineering, Adv. Phys. **64**, 139 (2015).
[40] N. R. Cooper, J. Dalibard, and I. B. Spielman, Topological bands for ultracold atoms, Rev. Mod. Phys. **91**, 015005 (2019).
[41] B. Wang, F. N. Ünal, and A. Eckardt, Floquet engineering of optical solenoids and quantized charge pumping along tailored paths in two-dimensional Chern insulators, Phys. Rev. Lett. **120**, 243602 (2018).
[42] M. Račiūnas, F. N. Ünal, E. Anisimovas, and A. Eckardt, Creating, probing, and manipulating fractionally charged excitations of fractional Chern insulators in optical lattices, Phys. Rev. A **98**, 063621 (2018).
[43] M. D. Reichl and E. J. Mueller, Floquet edge states with ultracold atoms, Phys. Rev. A **89**, 063628 (2014).
[44] L. J. Maczewsky, J. M. Zeuner, S. Nolte, and A. Szameit, Observation of photonic anomalous Floquet topological insulators, Nat. Commun. **8**, 13756 (2017).
[45] S. Mukherjee, A. Spracklen, M. Valiente, E. Andersson, P. Öhberg, N. Goldman, and R. R. Thomson, Experimental observation of anomalous topological edge modes in a slowly driven photonic lattice, Nat. Commun. **8**, 13918 (2017).
[46] J. C. Budich, Y. Hu, and P. Zoller, Helical Floquet channels in 1D lattices, Phys. Rev. Lett. **118**, 105302 (2017).
[47] P. Titum, E. Berg, M. S. Rudner, G. Refael, and N. H. Lindner, Anomalous Floquet-Anderson insulator as a nonadiabatic quantized charge pump, Phys. Rev. X **6**, 021013 (2016).
[48] C. Gross and W. S. Bakr, Quantum gas microscopy for single atom and spin detection, Nat. Phys. **17**, 1316 (2021), and references therein.
[49] A. Quelle, C. Weitenberg, K. Sengstock, and C. M. Smith, Driving protocol for a Floquet topological phase without static counterpart, New J. Phys. **19**, 113010 (2017).
[50] F. Nathan and M. S. Rudner, Topological singularities and the general classification of Floquet-Bloch systems, New J. Phys. **17**, 125014 (2015).
[51] See Supplemental Material at http://link.aps.org/supplemental/10.1103/PhysRevA.108.063314 for details.
[52] A. M. Kaufman and K. K. Ni, Quantum science with optical tweezer arrays of ultracold atoms and molecules, Nat. Phys. **17**, 1324 (2021), and references therein.
[53] C. Braun, R. Saint-Jalm, A. Hesse, J. Arceri, I. Bloch, and M. Aidelsburger, Real-space detection and manipulation of topological edge modes with ultracold atoms, arXiv:2304.01980.
[54] G. M. Nixon, F. N. Ünal, and U. Schneider, Individually tunable tunnelling coefficients in optical lattices using local periodic driving, arXiv:2309.12124.
[55] F. D. M. Haldane, Model for a quantum hall effect without landau levels: Condensed-matter realization of the "parity anomaly", Phys. Rev. Lett. **61**, 2015 (1988).
[56] J.-Y. Zhang, C.-R. Yi, L. Zhang, R.-H. Jiao, K.-Y. Shi, H. Yuan, W. Zhang, X.-J. Liu, S. Chen, and J.-W. Pan, Tuning anomalous Floquet topological bands with ultracold atoms, Phys. Rev. Lett. **130**, 043201 (2023).
[57] A. F. Adiyatullin, L. K. Upreti, C. Lechevalier, C. Evain, F. Copie, P. Suret, S. Randoux, P. Delplace, and A. Amo, Topological properties of Floquet winding bands in a photonic lattice, Phys. Rev. Lett. **130**, 056901 (2023).